

Examining Interfacial Diffuse Phonon Scattering Through Transient Thermoreflectance Measurements of Thermal Boundary Conductance

Pamela M. Norris¹

e-mail: pamela@virginia.edu

Patrick E. Hopkins²

Department of Mechanical and Aerospace
Engineering,
University of Virginia,
P.O. Box 400746,
Charlottesville, VA 22904-4746

Today's electronic and optoelectronic devices are plagued by heat transfer issues. As device dimensions shrink and operating frequencies increase, ever-increasing amounts of thermal energy are being generated in smaller and smaller volumes. As devices shrink to length scales on the order of carrier mean free paths, thermal transport is no longer dictated by the thermal properties of the materials comprising the devices, but rather the transport of energy across the interfaces between adjacent materials in the devices. In this paper, current theories and experiments concerning phonon scattering processes driving thermal boundary conductance (h_{BD}) are reviewed. Experimental studies of thermal boundary conductance conducted with the transient thermoreflectance technique challenging specific assumptions about phonon scattering during thermal boundary conductance are presented. To examine the effects of atomic mixing at the interface on h_{BD} , a series of Cr/Si samples was fabricated subject to different deposition conditions. The varying degrees of atomic mixing were measured with Auger electron spectroscopy. Phonon scattering phenomena in the presence of interfacial mixing were observed with the trends in the Cr/Si h_{BD} . The experimental results are reviewed and a virtual crystal diffuse mismatch model is presented to add insight into the effect of interatomic mixing at the interface. The assumption that phonons can only transmit energy across the interface by scattering with a phonon of the same frequency—i.e., elastic scattering, can lead to underpredictions of h_{BD} by almost an order of magnitude. To examine the effects of inelastic scattering on h_{BD} , a series of metal/dielectric interfaces with a wide range of vibrational similarity is studied at temperatures above and around materials' Debye temperatures. Inelastic scattering is observed and new models are developed to predict h_{BD} and its relative dependency on elastic and inelastic scattering events.

[DOI: 10.1115/1.3072928]

Keywords: thermal boundary conductance, pump probe transient thermoreflectance technique, diffuse phonon scattering, material diffusion, Auger electron spectroscopy, elemental characterization, elastic scattering, inelastic scattering, nanoscale solid-solid interfaces

1 Introduction

The ongoing trend of miniaturization on the nanoscale has created many new thermal challenges for device engineers and scientists. In many solid state devices, increased power densities in combination with continued size reductions are giving rise to thermal processes that cannot be predicted by traditional macroscopic laws and models. For example, as transistor gate lengths are continuously decreasing in an effort to continue the trends projected by Moore's law, power dissipation is becoming a growing concern. Moore's law is commonly reported as the doubling of transistor density on an integrated circuit (IC) every 18 months. As seen from the trends of the Intel® microprocessors since the turn of the 21st century, IC engineers have met and exceeded expecta-

tions of Moore's law [1]. Much of this progress is attributed to the ability of engineers and scientists to effectively manage the thermal issues that arise from the continued size reduction of the components in the ICs. However, in the most current and envisioned applications of nanostructures and nanodevices, thermal management is a serious issue that is impeding development and productivity [2].

With the continued reduction of feature sizes in these nanosystems, theories and predictions based on macroscopic principles must be abandoned in order to accurately deal with the thermal issues. This is a consequence of the characteristic lengths of materials in nanodevices reducing to sizes on the order of the mean free path, Λ , of the primary energy carriers in solids at device operating temperatures. As operating speeds increase, for example, the characteristic sizes of the transistors in the ICs are approaching dimensions on the order of 10 nm. Since multiple carrier-carrier scattering events do not occur when characteristic lengths are on the order of the mean free path, a local temperature gradient cannot be established, and therefore Fourier's law does not apply. This presents an increased challenge for managing the

¹Corresponding author.

²Present address: Engineering Sciences Center, Sandia National Laboratories, P.O. Box 5800, Albuquerque, NM 87185-0346.

Contributed by the Heat Transfer Division of ASME for publication in the JOURNAL OF HEAT TRANSFER. Manuscript received June 12, 2008; final manuscript received October 8, 2008; published online February 20, 2009. Review conducted by Robert D. Tzou. Paper presented at the 2008 International Conference on Macro/Nanoscale Heat Transfer (MNHT2008), Tainan, Taiwan, January 6–9, 2008.

energy transport in these devices, since ultimately, heat is undesirable and must be removed from the active regions of these devices that are generating energetic carriers.

Although this nanoscale size effect poses a major problem for understanding energy transfer through materials in a device [3,4], as these materials become smaller, more critical to the thermal management of many nanoscale devices is understanding how energy is transferred *across the interfaces* of the many materials that make up a device. As device dimensions shrink, it is becoming more likely that an energy carrier will scatter at an interface between two adjacent materials, where the resistance to energy transfer at this interface is much higher than in the materials that form the interface [2]. This thermal boundary resistance, R_{BD} (the inverse of thermal boundary conductance, h_{BD}), gives rise to a temperature drop, ΔT , across the interface of materials where energy transport occurs.

Thermal boundary conductance, sometimes termed Kapitza conductance, was first observed by Kapitza in 1941 [5] between copper and liquid helium by observing that in the presence of a heat flux across the copper/liquid helium boundary, a temperature discontinuity existed. This phenomenon can be caused by, for example, the differing transport properties of the materials adjacent to the interface [6] or a disordered region of the materials resulting from device fabrication conditions [7]. The thermal boundary conductance, h_{BD} , relates the heat flux to the temperature drop ΔT across the interface.

$$q = h_{BD}\Delta T \quad (1)$$

The consideration of h_{BD} is vital in the design of nanostructures used in, for example, IC design, thermal interface materials [8–10], thermoelectric devices [11,12], thin-film high temperature superconductors [13,14], vertical cavity surface emitting lasers [15], optical data storage media [16], ultrashort pulsed laser systems [17,18], and high power density field effect transistors [19,20].

In this paper, current theories and experiments concerning phonon scattering processes driving thermal boundary conductance (h_{BD}) are reviewed. Traditional models make assumptions about phonon scattering that limit their range of applicability. These models and assumptions are discussed in Sec. 2 along with the transient thermoreflectance (TTR) technique, a measurement technique common in measuring interfacial thermal conductance. The remainder of the paper will review experimental studies of thermal boundary conductance conducted with the TTR technique challenging specific assumptions about phonon scattering during interfacial heat transfer. The experimental results are summarized and several new models, developed as a result of these experiments, are reviewed.

2 Phonon Interfacial Transport: Theory and Measurements

Although much work has been done in the area of interfacial thermal transport, most of the work has been done at low temperatures (<10 K) and for liquid-solid interfaces. While there have been a few proposed theories for room temperature application, most of which are adaptations of the low temperature models, there is no model that reliably captures the variability in measured interfacial thermal conductance. An understanding of the basic transport mechanisms involved in interfacial transport is critical to the design and engineering of nanostructured material systems used in a wide range of technologies, from state-of-the-art nanoelectronics, to thermoelectric modules, to thermal barrier coatings used in turbine engines.

Thermal energy is transported in metallic materials nearly completely by the electron system, whereas in nonmetals, the energy is stored and transported by phonons. Phonon scattering, the main transport mechanism across a wide range of device interfaces, has been successfully predicted by various models in limiting cases. These models are based on the specular or diffuse nature of pho-

non scattering at the interface. When a phonon undergoes specular scattering, the angle of the incident phonon equals the reflected angle and the angle of the transmitted phonons can be determined by Snell's law. When a phonon undergoes diffuse scattering, the scattering event is completely independent of any information about the particle before the scattering event, such as the angle of incidence. The particle scatters with equal probability in all directions. The specular parameter, p , estimates the probability that phonons are specularly scattered [21];

$$p = \exp\left[-\frac{16\pi^2\delta^2}{\lambda^2}\right] \quad (2)$$

where δ is the roughness parameter and λ is the phonon wavelength. In the case of interfaces, the roughness parameter, δ , is the mean square deviation of the height of the surface from the reference plane [22]. A representative wavelength of the phonon system approaching the interface can be estimated by the thermal coherence length, \mathcal{L}_{th} , which assuming a thermal spread of $k_B T$, can be calculated by [22]

$$\mathcal{L}_{th} = \frac{2\pi\hbar v}{k_B T} \quad (3)$$

Here k_B is Boltzmann's constant, \hbar is Planck's constant, and v is the phonon group velocity. At low temperatures, \mathcal{L}_{th} is large and p approaches 1 (completely specular scattering). As temperature increases, \mathcal{L}_{th} decreases, which decreases the probability of specular scattering (increases the probability of diffuse scattering).

Specular scattering is most likely experienced by long wavelength phonons (which represent the majority of phonons that are excited at low temperatures) at perfectly smooth interfaces. For example, consider an acoustically hard material, such as diamond, at 5 K. The diamond phonons approach an interface with only one monolayer of roughness (the lattice constant of diamond is ≈ 3.57 Å). Given an average phonon velocity of $v_{\text{diamond}} = 14,367$ m s⁻¹ [23], a specular parameter of $p=0.997$ is calculated for the diamond phonon scattering. However, as temperature is increased up to 300 K, the specular parameter drops down to $p=0$, indicating that all phonons will undergo diffuse scattering events.

To predict h_{BD} in the event of purely specular scattering, Little proposed the acoustic mismatch model (AMM) [24,25]. In the AMM the transmissivity, that is, the percentage of the incident phonons that will be transmitted across the interface, is calculated based on the ratio of acoustic impedances of the materials on either side of the interface. The AMM has proven successful at predicting h_{BD} at low temperatures ($T < 7$ K) and at ideal interfaces [7]. However, this ideal case only represents a very limited population of interfaces in modern devices, which often operate at higher temperatures and have disordered regions near the interface that would induce diffuse scattering. To account for this type of phonon scattering, Swartz and Pohl [26] developed the diffuse mismatch model (DMM) to predict h_{BD} at more realistic interfaces.

To apply the DMM in its simplest form, the following assumptions must be made: (1) phonons are elastically scattered—i.e., a phonon from side 1 with frequency ω can only emit a phonon into side 2 with the same frequency ω after the scattering event (for discussions, side 1 will refer to the softer material with lower phonon velocities and side 2 will refer to the stiffer material with higher phonon velocities); (2) phonon scattering is completely diffuse—i.e., a scattered phonon has no memory of the mode (longitudinal or transverse) or direction of the incident phonon; and (3) the materials on both sides of the interface are elastically isotropic—i.e., the longitudinal and transverse acoustic velocities are constant in all crystallographic directions. The DMM is mathematically stated as

$$h_{BD}^{DMM} = \frac{1}{4} \sum_j \int_0^{\omega_j^c} v_{i,j} \hbar \omega D_{i,j}(\omega) \frac{\partial f^0(\omega, T)}{\partial T} \zeta^{i \rightarrow 3-i}(\omega) d\omega \quad (4)$$

where the transmissivity from side i to side $3-i$, $\zeta^{i \rightarrow 3-i}$, has no angular or phonon mode dependence because of the nature of diffuse scattering, $D(\omega)$ is the density of states, ω is the phonon frequency, and v is the phonon velocity. The generalized notation of superscript $3-i$ denotes the side opposite to side i , so that the side opposite to side 1 is 2 and the side opposite to side 2 is 1 [26]. The subscripts i and j refer to the side and the phonon mode (longitudinal or transverse), respectively, and the superscript 0 on f^0 refers to an equilibrium distribution. Diffuse scattering will rethermalize the phonon system (thermalizing black boundaries) [4] so the phonon system can be described by the equilibrium Bose–Einstein distribution ($f^0(\omega, T)$) and can therefore be characterized by a temperature at the interface, T . The cutoff frequency, ω^c , of each phonon mode j can be calculated for the separate phonon modes assuming an isotropic Debye solid, $\omega_j^c = v_j(6\pi^2 N)^{1/3}$, where N is the total number of phonons per unit volume [27]. Assuming a Debye density of states, the transmission probability is calculated by [26]

$$\begin{aligned} \zeta^{i \rightarrow 3-i}(\omega) &= \frac{\sum_j \frac{1}{v_{3-i,j}^2}}{\sum_j \frac{1}{v_{i,j}^2} + \sum_j \frac{1}{v_{3-i,j}^2}} = \frac{\frac{1}{v_{3-i,L}^2} + \frac{2}{v_{3-i,T}^2}}{\frac{1}{v_{i,L}^2} + \frac{2}{v_{i,T}^2} + \frac{1}{v_{3-i,L}^2} + \frac{2}{v_{3-i,T}^2}} \\ &= \zeta^{i \rightarrow 3-i} \end{aligned} \quad (5)$$

which is a result of applying the principle of detailed balance [28] to the phonon fluxes from sides i and $3-i$ approaching a perfect interface and assuming single phonon elastic scattering.

This model has been shown to predict conductance across higher temperature interfaces ($T > 15$ K) relatively well [7,26]. However, at much higher temperatures (such as the operating temperatures of high frequency microelectronic devices), the DMM has been shown to either underpredict or overpredict experimental data, depending on the material systems [6]. Neither the AMM and DMM accurately predict h_{BD} in most practical material systems at conditions of technological interest.

Another model for h_{BD} , the phonon radiation limit (PRL), estimates the maximum conductance for interfacial transport from elastic scattering [29]. Development of the PRL is very similar to that of the DMM. However, the PRL assumes that all of the phonons in side $3-i$ up to the cutoff frequency in side i (assuming $\omega_j^c < \omega_{3-i}^c$) contribute to thermal transport though elastic collisions ($\zeta^{3-i \rightarrow i} = 1$). With these assumptions, the PRL is given as

$$h_{BD}^{PRL} = \frac{1}{4} \sum_j \int_0^{\omega_{3-i,j}^c} v_{3-i,j} \hbar \omega D_{3-i,j}(\omega) \frac{\partial f^0(\omega, T)}{\partial T} d\omega \quad (6)$$

which represents the maximum conductance due to elastic scattering. Since the PRL represents the upper limit of the elastic contribution to thermal transport, it will always predict a higher h_{BD} than the DMM. The DMM and PRL predict a constant h_{BD} at temperatures approaching the Debye temperature, θ_D , of the lower Debye temperature material (acoustically “softer” material or the material with the lower phonon velocity). This has to do with the change in the phonon population of the metal film as a function of temperature, and the fundamental assumption of elastic scattering employed in the DMM and PRL.

3 Experimental Measurement of h_{BD} Using the Transient Thermoreflectance Technique

There are many different techniques that have been used to measure thermal boundary conductance. An in-depth review of these techniques put into historical context is given by Swartz and Pohl [26]. This paper reviews studies by several groups who have

used the TTR technique to measure h_{BD} for a wide range of material interfaces. The TTR technique employs a “pump” light pulse that is focused to a small spot on the surface of a metallic film that, upon absorption of the incident photons by the electrons in the metal, creates a temperature rise in the electron system. This change in temperature of the film produces a proportional change in the reflectivity. The change in the reflectivity as the film cools by conduction into the underlying structures is measured with a time-delayed “probe” light pulse, which is focused onto the center of the heated region of the film.

The experimental results presented here were obtained using the TTR experimental setup shown schematically in Fig. 1. The primary laser output emanates from a Coherent RegA 9000 amplifier (seeded with a Coherent MIRA 900 oscillator) operating at a 250 kHz repetition rate with about 4 μ J/pulse and a 150 fs pulse width at 800 nm (1.55 eV), which is split at a 9:1 pump to probe ratio. The pump beam, which is modulated at 125 kHz by an acousto-optic modulator (AOM), provides a modulated sequence of excitation events on the sample surface. The probe beam passes through a half-wave plate, rotating the polarization by 90 deg relative to the pump, which enables improved noise filtering. The length of the probe path is set by precise control of a dovetail prism mounted on a variable delay stage, with a total maximum delay between the pump and probe pulses of 1500 ps. The probe is directed through a polarizing filter, oriented such that only the probe light is passed and not the pump, which is positioned before a silicon photodiode, which monitors the reflection of the probe beam off the sample. A lock-in amplifier triggered at the modulation frequency of the pump monitors the photodiode response to the modulation in intensity of the probe beam. The radii of the pump and probe beams are measured with a sweeping knife edge technique [30]. Although the low repetition rate of the RegA system and the “one shot on–one shot off” modulation rate of the pump beam ensure minimal residual heating between pump pulses, the phase of the signal must still be taken into account to account for electronic noise. Phase correction is performed by the procedures for signal phase adjustment outlined by Stevens et al. [30]. The thermal boundary conductance is determined by fitting the TTR data to a lumped capacitance thermal model with h_{BD} as the free parameter, as outlined in Refs. [31,32].

4 Inability of the DMM to Accurately Predict h_{BD}

The TTR method has been used to determine h_{BD} on a wide variety of interfaces and experimental measurements show a wide range of agreement with the DMM. This is easily seen in Fig. 2, which shows the ratio of measured h_{BD} with the TTR technique to predict h_{BD} with the DMM calculated via Eqs. (4) and (5) as a function of the ratio of the materials’ Debye temperatures. The ratio of the two materials’ Debye temperatures gives a quantitative value to compare the degree of differing vibrational states between two materials. If the ratio is close to unity, then the materials have very similar cutoff frequencies, and are considered acoustically matched. If the ratio is much smaller or greater than unity, then the samples are considered acoustically mismatched.

Figure 2 clearly demonstrates the inability of the DMM to accurately predict h_{BD} . It is seen that in acoustically well-matched material systems with a Debye temperature ratio close to 1, the DMM overpredicts the boundary conductance while for mismatched systems the DMM underpredicts the conductance by as much as an order of magnitude. It should be noted, however, that the interfaces of these samples were not abrupt junctions, and the influence of the possible formation of a finite-size mixing or two-phase region at the interface could not be determined. This work investigates the underprediction and overprediction of the DMM by systematically investigating two effects, interatomic mixing and inelastic scattering. These investigations seek to further explore the validity of the *single phonon elastic scattering assumption*.

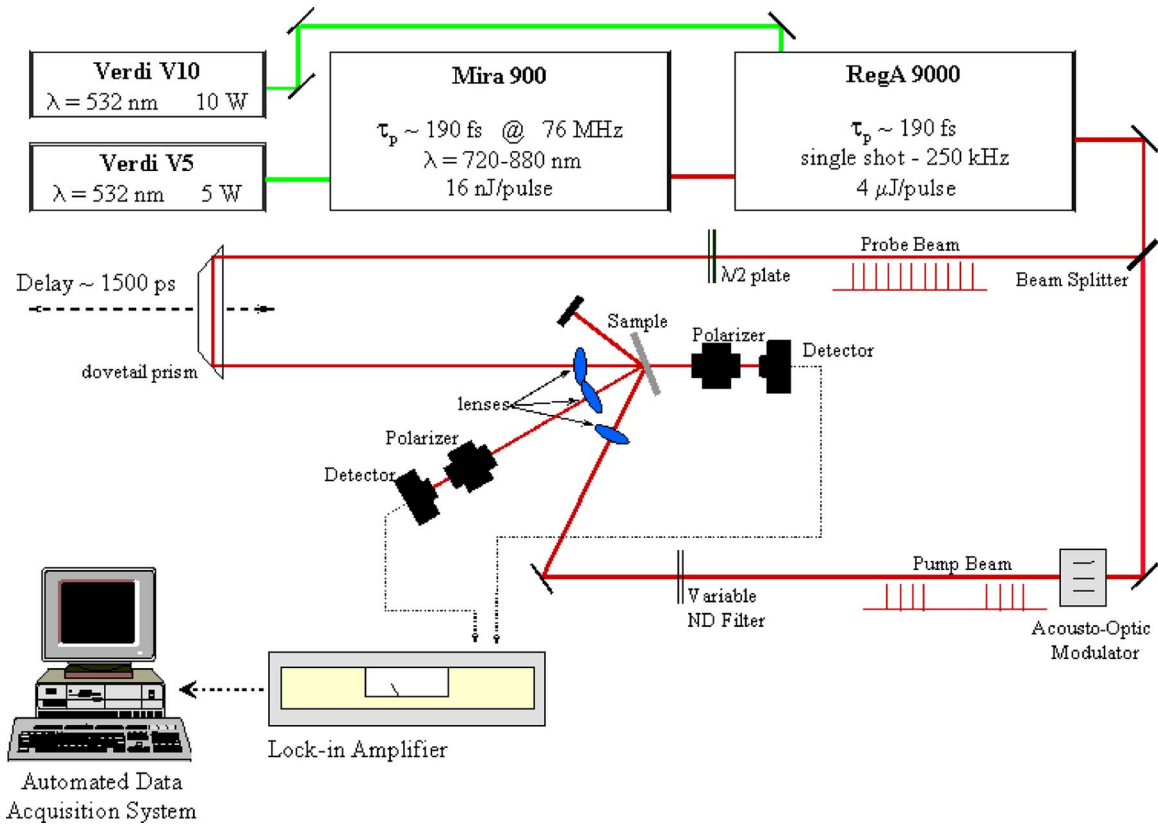


Fig. 1 Schematic of the transient thermoreflectance setup at the University of Virginia's Microscale Heat Transfer Laboratory

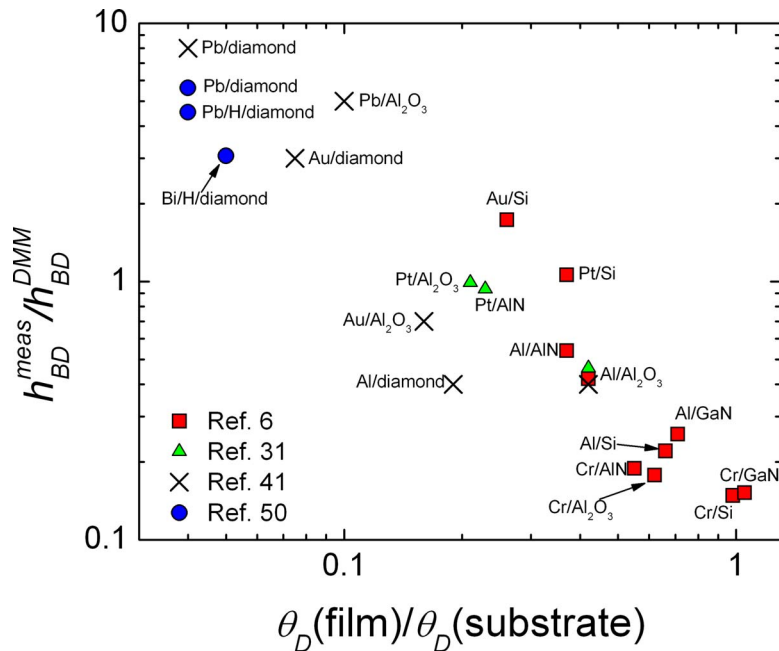


Fig. 2 Ratio of measured h_{BD} , h_{BD}^{meas} , to h_{BD} predicted from the DMM, h_{BD}^{DMM} , versus the ratios of the Debye temperatures of the metal film to the dielectric substrate. The data presented in this figure are selected results from Stevens et al. [6], Lyeo and Cahill [50], Stoner and Maris [41], and Hopkins et al. [31]. Some of the diamond substrates were subject to hydrogen termination before metal film deposition represented by the "H/diamond" after the metal film. The general trend shows that the DMM underpredicts measurements on acoustically mismatched samples and overpredicts measurements on acoustically matched samples.

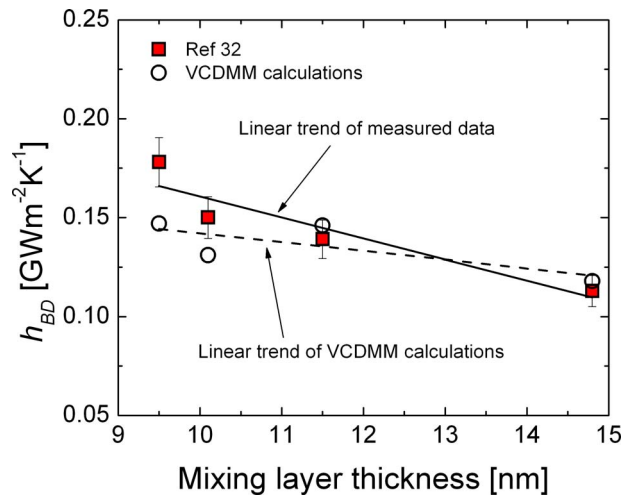


Fig. 3 Thermal boundary conductance measurements on various Cr/Si interfaces from Hopkins et al. [32] and corresponding VCDMM calculations from Beechem et al. [34]. Where the DMM predicts h_{BD} that is almost eight times larger ($0.86 \text{ GW m}^{-2} \text{ K}^{-1}$) than that measured on the samples with no dependence on mixing layer thickness or compositions, the VCDMM calculations are within 18% of the measured values and show similar trends with mixing layer thickness when taking into account the change in Si composition in the mixing region.

5 Effects of Interatomic Mixing on Thermal Boundary Conductance

In realistic nanodevices, pronounced interdiffusion or reactions at the interface can occur on the order of the characteristic length of the device, even at room temperature [33]. This interdiffusion results in the presence of a disordered and two-phase region at the interface of two materials, which contributes to the overall h_{BD} [26]. The effect of disorder, or a two-phase region, on h_{BD} has been the focus of many numerical studies [34–38], but the lack of experimental observation has led to conflicting theoretical results for h_{BD} as a result of multiphase and diffusion regions. For example, the scattering-mediated acoustic mismatch model, which assumes complete specular scattering, predicts a decrease in h_{BD} [39], while calculations by Kozorezov et al. [40] indicate an increase. Lattice dynamics calculations have offered insight into phonon interfacial transmission and h_{BD} , but these only apply to specific interfacial structures. There have been limited experimental studies on the role of mixing on h_{BD} , but the Norris Laboratory just recently was the first to publish quantitative experimental results relating thickness of the interdiffusion region to changes in measured h_{BD} [32].

Hopkins et al. [32] measured h_{BD} across different Cr/Si interfaces subjected to various fabrication conditions with the TTR technique. Chromium and Si represent acoustically matched materials with nearly identical Debye temperatures ($\theta_D(\text{Cr})=630 \text{ K}$ and $\theta_D(\text{Si})=640 \text{ K}$) [27] and therefore have similar cutoff frequencies. The interfaces were characterized with Auger electron spectroscopy (AES) to quantify the thickness of material mixing and elemental concentration in the mixing region. The interfacial mixing observed in these AES profiles ensures completely diffuse scattering, so the DMM can be compared with the experimental data. The DMM predicts h_{BD} of $0.855 \text{ GW m}^{-2} \text{ K}^{-1}$ using a Debye approximation. The measured h_{BD} ranged from $0.178 \text{ GW m}^{-2} \text{ K}^{-1}$ in the sample with a 9.5 nm mixing layer thickness to $0.113 \text{ GW m}^{-2} \text{ K}^{-1}$ in the sample with 14.8 nm of mixing as shown in Fig. 3. The DMM overpredicts the measured h_{BD} , which has often been associated with poor interface quality and substrate damage [6,7,26,41].

A portion of the difference between the measured h_{BD} and that calculated from the DMM in well-matched samples such as Cr/Si could result from varying degrees of mixing. The DMM does not take into account an interfacial mixing layer. Although the scattering-mediated acoustic mismatch model accounts for multiple scattering events that could result from interfacial disorder [39], it assumes specular phonon reflection, which clearly is not a valid assumption in this case since the interfacial region was observed to be significantly disordered.

At an ideal interface with no mixing, a phonon from the Cr film scatters at the Cr/Si interface, and is either transmitted into the Si or reflected back into the Cr. From Eq. (5) the phonon transmission probability for the Cr/Si interface is $\zeta^{\text{Cr} \rightarrow \text{Si}}=37\%$, meaning that at the ideal interface, 37% of the phonons are transmitted from the Cr into the substrate. In the event of interfacial mixing, the phonons must propagate across a finite amount of space to conduct energy into the substrate. When these phonons scatter with Si at the beginning of the mixing layer, a certain percentage of the phonons are transmitted deeper into the mixing layer. As the thickness of the interfacial mixing layer increases, the probability that a phonon will scatter more than once increases thereby decreasing h_{BD} , which is expected with increased diffuse scattering in well-matched materials. Thus, the presence of an interfacial mixing region causing multiple elastic scattering events, which are not accounted for, may be the cause of the overestimation of the DMM in well-matched material systems with Debye temperature ratios close to 1.

6 Predicting the Interfacial Mixing Dependency of h_{BD} With the VCDMM

Beechem et al. [34] presented a virtual crystal diffuse mismatch model (VCDMM) to predict the influence of mixing region thickness and composition on h_{BD} . This model introduces a simple correction to the DMM through use of a virtual crystal to account for the manner by which energy propagates through the interfacial region. In this manner multiple scattering events occurring at the interface can be quantified allowing for more accurate prediction of h_{BD} as well as insight into the effect of interfacial quality on overall heat transfer.

To account for a finite interfacial thickness, the VCDMM replaces the interfacial region with a third material, the virtual crystal, which has properties that are a blend of the bulk materials on either side [42] and a thickness equal to the length of disorder. Incorporating the virtual crystal modifies the DMM to account for both the interaction between each of the bulk materials and interface as well as the now finite thickness of the interface.

The interaction between the two materials and the disordered region is investigated by estimating the conductance between each of the bulk materials and the virtual crystal. This is accomplished by applying the DMM for each of the now two interfaces with a modification of the transmission coefficient to account for the virtual crystal so that the transmission is calculated at the i /virtual crystal and $3-i$ /virtual crystal interfaces. Again, this calculation assumes all solids are Debye solids. It follows that h_{BD} for the two-interface system is given by

$$h_{BD}^{\text{VCDMM}} = \left[\frac{1}{h_{BD}^{i \rightarrow \text{VC}}} + \frac{1}{h_{BD}^{3-i \rightarrow \text{VC}}} \right]^{-1} \quad (7)$$

The above relation accounts for only the efficiency by which energy transfers from the bulk to the interface but does not analyze the ease by which energy propagates through the interfacial region. To examine this effect, the results of Eq. (7) are scaled according to the depth factor, Ξ , which is a ratio of the interfacial thickness, δ , to the mean free path of the virtual crystal, Λ_{VC} ($\Xi = \delta/\Lambda_{\text{VC}}$). The interfacial thickness, δ , is also the roughness parameter used in Eq. (2). Using kinetic theory with the virtual crystal approximation for thermal conductivity [42] to estimate

the mean free path along with the measured thickness of the Cr/Si interface, the depth factor is calculated allowing for the estimation of h_{BD} from the VCDMM by

$$h_{BD}^{VCDMM} = \left[\frac{\Xi}{h_{BD}^{i \rightarrow VC}} + \frac{\Xi}{h_{BD}^{3-i \rightarrow VC}} \right]^{-1} = \frac{\Lambda_{VC}}{\delta} \left[\frac{1}{h_{BD}^{i \rightarrow VC}} + \frac{1}{h_{BD}^{3-i \rightarrow VC}} \right]^{-1} \quad (8)$$

Equation (8) describes the effect of interatomic mixing around the interface on phonon interfacial transport. However, in acoustically matched metal/dielectric material systems such as Cr/Si, another channel of energy transport associated with electron-phonon nonequilibrium could significantly affect interfacial energy transport [43]. In well-matched material systems, the thermal resistance associated with phonon-phonon interfacial transport, $R_{pp} = 1/h_{pp}$, is relatively small and on the same order as the resistance associated with an electron-phonon nonequilibrium in the film near the interface, $R_{ep} = 1/h_{ep}$, where this electron-phonon boundary conductance is given by [43]

$$h_{ep} = \sqrt{k_{pp}G} \quad (9)$$

where k_{pp} is the phonon thermal conductivity in the metal and G is the electron-phonon coupling factor of the metal [44–47]. Therefore, in acoustically matched material systems, R_{ep} must also be taken into account, which leads to

$$h_{BD}^{VCDMM} = \left\{ \frac{1}{\sqrt{k_{pp}G}} + \Xi_j \left[\frac{1}{h_{BD}^{i \rightarrow VC}} + \frac{1}{h_{BD}^{3-i \rightarrow VC}} \right] \right\}^{-1} \quad (10)$$

Shown in Fig. 3 is a comparison of the virtual crystal model to the experimental data from Hopkins et al. [32]. The virtual crystal approach is within 18% of the measured values whereas the predicted h_{BD} of the DMM, which does not account for any interfacial mixing, is about eight times these values. In both prediction and measurement, there is a distinct trend of decreasing h_{BD} with increasing interfacial thickness. This results from the additional scattering, which occurs as the phonons must propagate through the disordered region.

7 Influence of Inelastic Phonon Scattering on Thermal Boundary Conductance

In an attempt to investigate the underpredictive trends of the DMM as seen in Fig. 2, several computational and experimental efforts have been undertaken. In 1993, Stoner and Maris [41] reported h_{BD} at a range of acoustically mismatched interfaces from 50 K to 300 K. As expected from the DMM, the measured h_{BD} decreased with an increase in sample mismatch and the change in h_{BD} decreased with temperature. In the sample with the greatest mismatch, Pb/diamond, values of h_{BD} were measured that exceeded the DMM prediction by two orders of magnitude. One possible explanation offered for the underestimate of h_{BD} by the DMM was the occurrence of inelastic scattering—i.e., one or more phonons of frequency ω_1 on side 1 were emitting one or more phonons of frequency ω_2 on side 2—thereby offering additional channels for transport not accounted for in the DMM. At a Pb/diamond interface, a high frequency diamond phonon could scatter at the interface and emit low frequency phonons on the Pb side.

As the interface temperature increases above the Debye temperature of the softer material (i.e., in the classical limit), the DMM predicts that h_{BD} is relatively constant. This is a result of the change in phonon population with temperature predicted by the Bose–Einstein distribution function. At temperatures close to a material's Debye temperature, the change in phonon population with temperature becomes linear. The DMM is a function of the temperature derivative of the Bose–Einstein distribution, which results in the constant h_{BD} predicted at higher temperatures (T

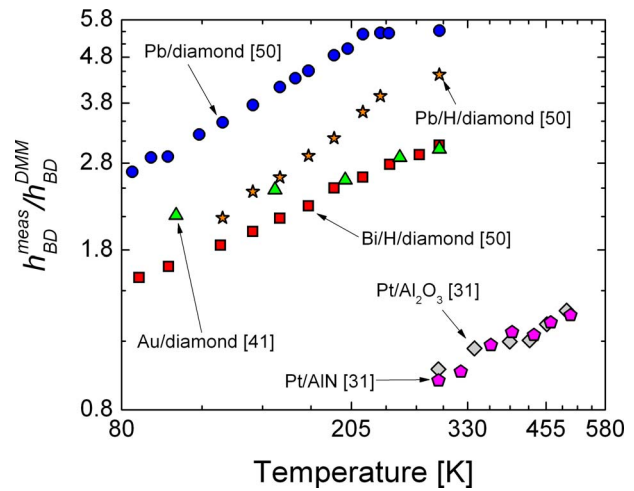


Fig. 4 Ratio of measured h_{BD} , h_{BD}^{meas} , to h_{BD} predicted from the DMM, h_{BD}^{DMM} , versus temperature for six different acoustically mismatched samples. The data presented in this figure are selected results of Lyeo and Cahill [50], Stoner and Maris [41], and Hopkins et al. [31]. Some of the diamond substrates were subject to hydrogen termination before metal film deposition represented by the H/diamond. The general trend shows that the increase in h_{BD} observed with temperature over the temperature range for each sample is much greater than the increase with temperature predicted by the DMM. These data show a linear trend in h_{BD} with temperature, which is evidence of inelastic scattering.

$> \theta_D$) when elastic scattering is assumed. Assuming only elastic scattering and a Debye solid, the transmission coefficient is independent of temperature.

To check the temperature dependence of h_{BD} , Stevens et al. [37] performed molecular dynamics (MD) simulations at a range of temperatures. The simulations were conducted on both highly and lightly mismatched interfaces with Debye temperature ratios of 0.2 and 0.5. A strong linear relationship was observed in the h_{BD} results for the temperature range considered, with h_{BD} varying by nearly a factor of 4. This strong linear temperature dependence suggests a thermal transport mechanism that is dependent on temperature in the classical limit. The most likely explanation for this discrepancy is that while MD simulation accounts for both elastic and inelastic scattering at the interface, the DMM accounts only for elastic scattering. Chen et al. [48] used MD simulations to examine a Kr/Ar nanowire interface, showing a linear increase in h_{BD} with an increase in temperature from 35 K to 55 K, which they ascribed to anharmonic processes. Kosevich [49] considered the role of inelastic scattering on the phonon transmission probability using a multiharmonic model to show that inelastic scattering makes a greater contribution to h_{BD} than elastic scattering for interfaces with very different vibrational spectra.

Evidence of inelastic scattering has been observed experimentally by Lyeo and Cahill [50] at low temperatures ($T \leq T_{room}$) and Hopkins et al. [31] at high temperatures ($T \geq T_{room}$). Lyeo and Cahill [50] observed an approximately linear increase in h_{BD} over a temperature range of 80–300 K on carefully prepared Pb and Bi thin films on diamond substrates. Hopkins et al. [31] observed a linear trend in h_{BD} over temperatures from 300 K to 500 K on several different samples, including the heavily mismatched Pt/Al₂O₃ and Pt/AlN interfaces. The linear trends observed in these experimental works match the aforementioned simulation results, which suggested that multiple-phonon processes (inelastic scattering) can play a significant role in interface thermal conductance. However, these data do not agree with the trends predicted by the DMM. Selected data from Stoner and Maris [41], Lyeo and Cahill [50], and Hopkins et al. [31] are shown in Fig. 4, which

shows the ratio of measured h_{BD} to that predicted from the DMM for six different samples over a 200 K temperature range. It is apparent that in these mismatched samples, the measured data show an increasing linear trend, which is much greater than the slightly increasing if not constant predictions from the DMM.

The presence of inelastic scattering events, which add an additional channel of interfacial energy transport, may be the cause of the underestimation of the DMM in mismatched material systems with distinctly different Debye temperatures. In well-matched material systems, such as Cr/Si as previously studied, the difference between the modes in the film and substrate is very small, so the joint vibrational modes near the interface are most likely present in both the film and substrate making elastic scattering highly probable.

8 Joint Frequency Diffuse Mismatch Model

An underlying assumption governing the DMM is that a phonon transmits energy across an interface by emitting a phonon with the same frequency, i.e., the phonons are elastically scattered. Therefore, as the interface temperature increases above the Debye temperature of the softer material, the DMM predicts that h_{BD} is relatively constant. This implies that the DMM predicts a constant h_{BD} above ~ 100 K for Pb/diamond since $\theta_D(\text{Pb})=105$ K [27]. In fact, the DMM predicts a constant h_{BD} above 100 K for any Pb interface regardless of the substrate. However, if inelastic phonon processes occur (i.e., a phonon with frequency $\omega_{\text{diamond}}^c$ scatters into several phonons with frequencies below ω_{Pb}^c), then the change in h_{BD} with temperature would be related to the change in the diamond phonon population in addition to the Pb population.

Hopkins and Norris [51] developed a simple correction to the DMM to account for the discrepancy between the DMM and the experimental data in the event of inelastic scattering. By blending the vibrational spectra of the film and substrate materials, an approximation for the contribution of the inelastic modes was developed with a diffuse scattering assumption, the joint frequency diffuse mismatch model (JFDMM). The JFDMM assumes the same form as the DMM but uses a modified phonon velocity that is taken as a weighted average of the velocities of the phonon systems from sides 1 and 2. Consequently, this results in a weighted average of the phonon spectra used in the h_{BD} calculation, given by

$$D_{\text{mod},j} = \frac{\omega^2}{2\pi^2 v_{\text{mod},j}^3}, \quad \omega \leq \omega_{\text{mod},j}^c \quad (11)$$

$$\omega_{\text{mod},j}^c = v_{\text{mod},j} \{6\pi^2 (\xi_i N_i + \xi_{3-i} N_{3-i})\}^{1/3} \quad (12)$$

$$v_{\text{mod},j} = \xi_i v_i + \xi_{3-i} v_{3-i} \quad (13)$$

where the weighting factor ξ_i is simply a percentage of the composition of the phonons in each material in the unit volume, expressed mathematically as

$$\xi_i = \frac{\frac{N_i}{N_{3-i}} M_i}{\frac{N_i}{N_{3-i}} M_i + M_{3-i}} \quad (14)$$

where M_i is the atomic mass of side i . Since the DMM is calculated per unit volume, to better estimate the percent composition of the joint vibrating atoms near the interface, the relative number of phonons on each side must be taken into account by including the number of oscillators per unit volume, N . This is similar to calculating the percent composition of atoms in any compound (for example, the %O in H₂O). This approximation introduces high frequency phonons that are available in the vibrational spectrum in side 2 (stiffer material or the substrate in the aforementioned data) but not side 1 (softer material or the film in the aforementioned data) into the incident heat flux. The JFDMM

increases the prediction of h_{BD} by a factor that is proportional to the side 2 vibrational spectrum, giving an approximation for inelastic scattering. The transmission coefficient for the JFDMM is still assumed to be calculated with Eq. (5); note that this relaxes the assumption of detailed balance since the JFDMM assumes a modified phonon flux.

Figure 5 compares the predictions from the DMM and JFDMM to experimental TTR data shown in Fig. 4. Figure 5 shows the ratio of measured h_{BD} to the predicted h_{BD} by the DMM and JFDMM. This figure compares predictive trends for data on Pt/AlN [31], Pt/Al₂O₃ [31], Au/diamond [41], Bi/H/diamond [50], and Pb/diamond and Pb/H/diamond [50]. The model calculations use elastic constants to calculate phonon velocities and material properties to calculate the cutoff frequencies [23]; the material properties used in these calculations are listed in Table 1. The ratio of measured data to DMM predictions is shown by the filled symbols and the ratio of measured data to the JFDMM is represented by the outline of the symbols with no fill. Note that the models cannot distinguish between different depositions or interface conditions [32,52], so the predictions by the models on the hydrogen terminated diamond and non-hydrogen-terminated substrates are the same. The JFDMM predicts a closer value and better temperature dependent trend to the experimental data than the DMM. The JFDMM shows a different temperature dependent trend than the DMM, which is more in line with the experimental data since it assumes that phonons with frequencies higher than the cutoff frequency in side 1 can participate in h_{BD} . These data sets represent material systems that show evidence of inelastic scattering at these temperatures. The agreement between the JFDMM and the experimental data is much closer in the heavily mismatched materials than the not-as-heavily mismatched materials. This could be due to the contributions of inelastic scattering to h_{BD} being much greater in the heavily mismatched material systems [53].

9 Inelastic and Elastic Scattering Contributions to Thermal Boundary Conductance

Although the JFDMM shows improvement in h_{BD} predictions in the event that inelastic phonon scattering dominates interfacial transport, this method makes necessary assumptions about phonon transport that deserve further attention. The main assumption of the JFDMM is that a fraction of the available phonon states in the substrate are present in the film. In actuality, the atoms around the interface are vibrating at joint modes by Newton's law of motion [54]. The maximum allowable frequency for these joint modes is the substrate cutoff frequency. However, dampening of these modes will occur due to the differing interatomic forces of the film and substrate. This prevents the joint modes from oscillating at certain frequencies. This continuum phenomenon is paralleled quantum mechanically in the JFDMM through the weighted average of the two materials' phonon states in the incident flux. The weighting factor, ξ , reflects the dampening of the substrate modes, and is used to enhance the incident phonon flux to take into account the joint vibrations that are allowed after dampening effects. However, without computationally expensive computer simulations or a rigorous theoretical treatment, this weighting factor cannot be explicitly determined for every phonon mode, and therefore should be viewed as an estimation of the joint modes participating in h_{BD} . The JFDMM can be viewed as a starting point for estimating the maximum h_{BD} due to inelastic scattering.

Consider atoms vibrating at joint modes around the interface with no dampening effects. These atoms can therefore vibrate at all allowable frequencies up to the maximum allowed frequency in the substrate. Atoms on sides 1 and 2 will be coupled in joint vibrational modes with frequencies up to the cutoff frequency of side 2. This is paralleled in the JFDMM by making the weighting factors (Eq. (14)) $\xi_1=0$ and $\xi_2=1$, which conceptually is treating h_{BD} as a function of the incident phonon flux from side 2 transmitted into side 1. This simplifies Eqs. (11)–(13) to $D_{\text{mod},j}=D_{2,j}$.

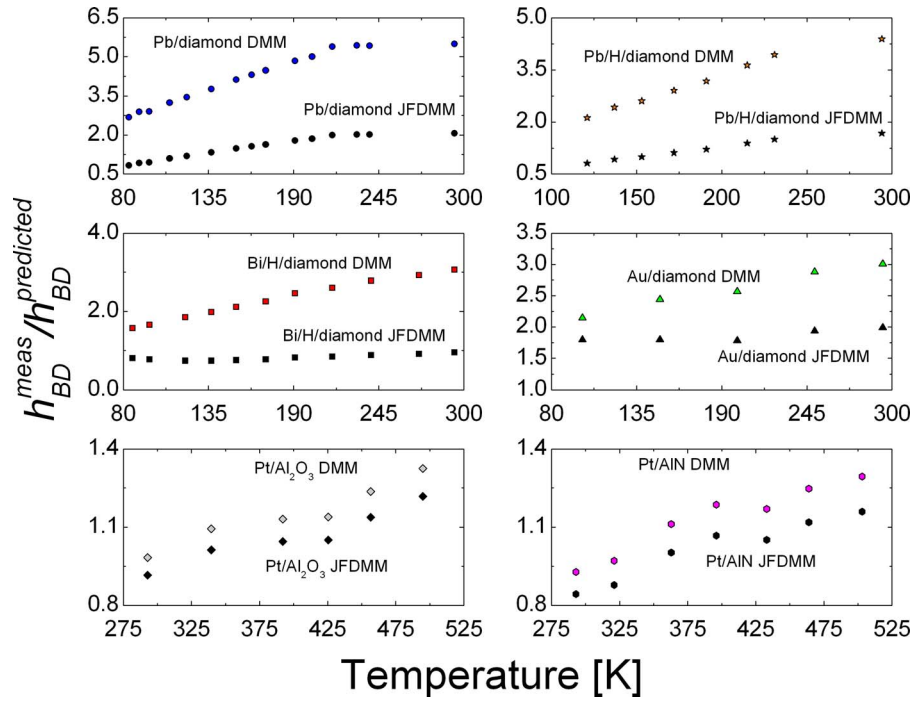


Fig. 5 Ratio of measured h_{BD} , h_{BD}^{meas} , to h_{BD} predicted from the DMM and JFDMM versus temperature for six different acoustically mismatched samples. The data presented in this figure are selected results of Lyeo and Cahill [50], Stoner and Maris [41], and Hopkins et al. [31]. The JFDMM captures the temperature trends in the data that exhibit inelastic scattering, and predicts h_{BD} values that are more in line with the experimental measurements.

$\omega_{\text{mod},j}^c = \omega_{2,j}^c$, and $v_{\text{mod},j} = v_{2,j}$, respectively, and redefines Eq. (4) in terms of the flux transmitted from side 2 to side 1, given as [53]

$$h_{BD}^{\text{inel}} = \frac{1}{4} \sum_j \int_0^{\omega_{2,j}^c} v_{3-i,j} \hbar \omega D_{3-i,j}(\omega) \frac{\partial}{\partial T} [J^0(\omega, T) \zeta_{3-i}^{\text{inel}}(T)] d\omega \quad (15)$$

From the nature of diffuse scattering, the inelastic transmission probability is $\zeta_2^{\text{inel}}(T) = 1 - \zeta_1^{\text{inel}}(T)$, which is different from the elastic transmission probability calculated with Eq. (5). Equation (15) allows higher frequency phonons that do not exist in the film to participate in h_{BD} . Without knowledge of the explicit temperature dependence of $\zeta_2^{\text{inel}}(T)$, h_{BD} cannot be calculated. However, the use of Eq. (15) along with experimental data can give important insights into the role of inelastic phonon scattering in thermal boundary conductance.

Hopkins and Norris [53] used Eq. (15) to develop the inelastic phonon radiation limit (IPRL). Consider the case where all available substrate phonons are participating in h_{BD} . In this case, the probability that a phonon on side 2 is inelastically transmitted

(i.e., scatters into lower frequency phonons and is transmitted into side 1) is unity. By letting $\zeta_2^{\text{inel}}(T) = 1$, Eq. (15) becomes an expression for the largest allowable thermal boundary conductance due to inelastic scattering, or the IPRL, expressed as

$$h_{BD}^{\text{IPRL}} = \frac{1}{4} \sum_j \int_0^{\omega_{2,j}^c} v_{2,j} \hbar \omega D_{2,j}(\omega) \frac{\partial f^0(\omega, T)}{\partial T} d\omega \quad (16)$$

The IPRL assumes that all side 2 phonons are transmitted into the film, and does not explicitly take into account elastic or inelastic scattering processes. However, by allowing all frequencies of phonons in side 2 to transmit energy into side 1, which has the lower cutoff frequency, inelastic scattering is implied. Note that in this limit, similar to the JFDMM, which also takes into account some inelastic scattering, the assumption of equilibrium is relaxed and therefore the principle of detailed balance is not enforced.

From the trends in the IPRL as compared with the PRL and experimental data, the relative contributions of elastic and inelastic scattering can be examined [53]. Above the film's Debye temperature, it is apparent that contributions from elastic scattering

Table 1 Pertinent thermophysical properties of materials in this work: from top to bottom: molar mass— M [23], molar density— n [23], longitudinal and transverse phonon velocities (which were calculated from the elastic lattice constants), v_L and v_T [23], Debye temperature— θ_D [27], and mass density— ρ [23]

	Al ₂ O ₃	AlN	Au	Bi	Cr	Diamond	Pb	Pt	Si
M (kg mol ⁻¹)	0.102	0.0203	0.197	0.209	0.052	0.012	0.207	0.195	0.028
n (mol m ⁻³)	38,922	160,345	97,970	46,794	138,269	290,008	55,990	110,872	83,214
v_L (m s ⁻¹)	10,890	11,120	3,390	1,543	6,980	17,500	2,350	4,174	8,970
v_T (m s ⁻¹)	6,450	6,267	1,290	1,107	4,100	12,800	970	1,750	5,332
θ_D (K)	1,043	1,150	165	119	630	2,230	105	240	645
ρ (kg m ⁻³)	3,970	3,255	19,300	9,780	7,190	3,512	11,590	21,620	2,330

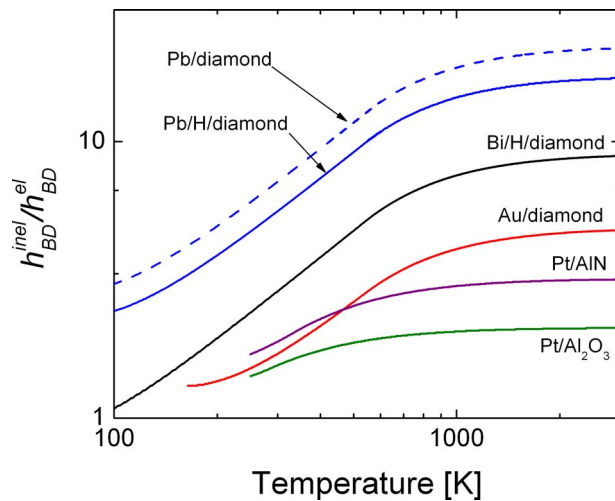


Fig. 6 Relative magnitude of inelastic scattering on h_{BD} . This ratio compares the inelastic contribution to h_{BD} to the elastic contribution. Details of these calculations are found in Ref. [53]. The role of inelastic phonon scattering increases as the acoustic mismatch of the film and substrate becomes greater. The range in which h_{BD} should increase linearly with temperature due to inelastic scattering also increases with acoustic mismatch.

will result in a constant h_{BD} . However, inelastic scattering events will drive the linear trend in h_{BD} . Therefore, the total thermal boundary conductance in the classical limit ($T > \theta_D$) will be a blend of both the constant elastic contribution and the temperature dependent inelastic phonon scattering contributions. To demonstrate the relative contribution to h_{BD} due to inelastic scattering as compared with that due to elastic scattering, the ratio $h_{BD}^{inel}/h_{BD}^{el}$ is plotted versus temperature in the classical regime in Fig. 6 for the six interfaces studied. As expected, the inelastic contributions compared with the elastic contributions to h_{BD} in Pb, Bi, and Au on diamond are more temperature dependent than the relative contribution in the Pt/Al₂O₃ and Pt/AlN samples due to the higher Debye temperature of diamond than Al₂O₃ and AlN. This also leads to the inelastic contributions becoming independent of temperature at higher temperatures in the diamond samples as compared with the Al₂O₃ and AlN substrate samples. In fact, the high temperature limits of the diamond substrate samples are not reached until the interface temperatures are driven above the melting temperature of the metal, meaning that in nanostructures composed of these interfaces, h_{BD} will continually increase with temperature until melting. Also, in the high temperature limit, as the mismatch between the materials adjacent to the interface grows, the contributions of inelastic phonon scattering to thermal boundary conductance increase.

10 Conclusions

The ongoing trend of miniaturization on the nanoscale has created many new thermal challenges for device engineers and scientists. An understanding of nanoscale energy transport is becoming increasingly important as standard device sizes continually decrease and classical heat transfer laws fail to predict energy transfer processes in a growing number of nanodevices. In nanodevices, it is more likely that energy carriers will scatter at an interface between two adjacent materials, where the resistance to energy transfer is much higher, than in the materials that form the interface. Traditionally used models do not adequately predict the rate of energy transfer across these interfaces, which is governed by the thermal boundary conductance, h_{BD} . The most commonly used model of h_{BD} , the DMM, overpredicts h_{BD} in well-matched material systems with a Debye temperature ratio close to 1 and

underpredicts h_{BD} for mismatched material systems by as much as an order of magnitude. The major limiting assumptions in the DMM are examined using experimental results obtained using the TTR technique, and several new models are presented.

A study of the interfacial transport in the presence of atomic mixing at the boundary between two materials lends insights into the effect of multiple-phonon scattering. The presence of an interfacial mixing region causing multiple elastic scattering events that are not accounted for may be the cause of the overestimation of the DMM in well-matched material systems with Debye temperature ratios close to 1. The VCDMM, which introduces a mixing region to the DMM, offers insight into the scattering processes that affect h_{BD} at these imperfect interfaces.

Experimental measurements of h_{BD} at elevated temperatures ($T \geq \theta_D$) enable exploration of the influence of inelastic scattering mechanisms. A linear trend in h_{BD} has been observed in several samples, even when the temperature is driven above the Debye temperature of the softer film material. Since the DMM only accounts for elastic scattering, the h_{BD} calculations from the DMM predict a relatively constant temperature trend. The measured linear trend shows that inelastic scattering contributes to interfacial transport at temperatures around and above the Debye temperature of a material adjacent to a solid interface.

To further understand the role of inelastic and elastic scattering events in interfacial transport, the JFDMM was developed, which takes into account the contributions of inelastic scattering to h_{BD} by considering the phonon flux at the interface to consist of frequencies that exist in both solids. The JFDMM shows improved values and trends in h_{BD} predictions from the DMM. From the basic assumptions of the JFDMM, an upper limit to h_{BD} was derived assuming all phonons are participating in energy transfer through inelastic scattering—the IPRL. To further understand inelastic scattering, experimental data on several interfaces were quantitatively compared, and the relative contributions of inelastic and elastic scattering to h_{BD} at these different interfaces were observed. The relative contribution of inelastic scattering to h_{BD} decreases as the materials adjacent to the interface become vibrationally similar.

Acknowledgment

The authors gratefully acknowledge financial support from the Office of Naval Research MURI program, Grant No. N00014-07-1-0723. P.E.H. also gratefully acknowledges support from the NSF Graduate Student Research Program.

Nomenclature

- D = spectral phonon density of states per unit volume
- f = phonon statistical distribution of energy states
- G = electron-phonon coupling factor, $\text{W m}^{-3} \text{K}^{-1}$
- \hbar = Planck's constant divided by 2π , J s
- h_{BD} = thermal boundary conductance, $\text{W m}^{-2} \text{K}^{-1}$
- k_B = Boltzmann's constant, J K^{-1}
- \mathcal{L}_{th} = thermal coherence length, m
- M = molar mass, kg mol^{-1}
- N = phonon number density, m^{-3}
- n = molar density, mol m^{-3}
- p = specular parameter
- R_{BD} = thermal boundary resistance, $\text{W}^{-1} \text{m}^2 \text{K}^1$
- T = temperature, K
- v = group velocity, m s^{-1}

Greek Symbols

- δ = interfacial roughness (thickness), m
- θ_D = Debye temperature, K
- ζ = interfacial transmission probability
- Λ = mean free path, m
- λ = wavelength, m

- ρ = mass density, kg m⁻³
 Ξ = interfacial depth factor
 ω = angular frequency of vibration, s⁻¹
 ξ = weight factor for vibrational states

Subscripts

- ep* = due to electron-phonon scattering
i = side *i*
j = polarization (longitudinal or transverse)
L = longitudinal mode
mod = modified to account for joint vibrational states
pp = due to phonon-phonon scattering
T = transverse mode

Superscripts

- 0 = equilibrium
c = cutoff
DMM = calculated with the diffuse mismatch model
el = accounting for elastic processes
i→3-*i* = from side *i* to side 3-*i*
i→VC = from side *i* to the virtual crystal
inel = accounting for inelastic processes
IPRL = calculated with the inelastic phonon radiation limit
meas = measured with the TTR technique
PRL = calculated with the phonon radiation limit
VCDMM = calculated with the virtual crystal diffuse mismatch model

References

- [1] Foster, L. E., 2006, *Nanotechnology: Science, Innovation, and Opportunity*, Pearson Education, Inc., Upper Saddle River, NJ.
[2] Cahill, D. G., Ford, W. K., Goodson, K. E., Mahan, G. D., Majumdar, A., Maris, H. J., Merlin, R., and Phillpot, S. R., 2003, "Nanoscale Thermal Transport," *J. Appl. Phys.*, **93**, pp. 793–818.
[3] Tien, C. L., Majumdar, A., and Gerner, F. M., 1998, *Microscale Energy Transport*, Taylor and Francis, Washington, DC.
[4] Majumdar, A., 1993, "Microscale Heat Conduction in Dielectric Thin Films," *ASME J. Heat Transfer*, **115**, pp. 7–16.
[5] Kapitza, P. L., 1941, "The Study of Heat Transfer in Helium II," *Zh. Eksp. Teor. Fiz. Pis'ma Red.*, **11**, pp. 1–31.
[6] Stevens, R. J., Smith, A. N., and Norris, P. M., 2005, "Measurement of Thermal Boundary Conductance of a Series of Metal-Dielectric Interfaces by the Transient Thermoreflectance Technique," *ASME J. Heat Transfer*, **127**, pp. 315–322.
[7] Swartz, E. T., and Pohl, R. O., 1987, "Thermal Resistances at Interfaces," *Appl. Phys. Lett.*, **51**, pp. 2200–2202.
[8] Chung, D. D. L., 2001, "Thermal Interface Materials," *J. Mater. Eng. Perform.*, **10**, pp. 56–59.
[9] Prasher, R. S., 2006, "Thermal Interface Materials: Historical Perspective, Status, and Future Directions," *Proc. IEEE*, **94**, pp. 1571–1586.
[10] Singhal, V., Siegmund, T., and Garimella, S. V., 2004, "Optimization of Thermal Interface Materials for Electronics Cooling Applications," *IEEE Trans. Compon. Packag. Technol.*, **27**, pp. 244–252.
[11] Da Silva, L. W., and Kaviany, M., 2004, "Micro-Thermoelectric Cooler: Interfacial Effects on Thermal and Electrical Transport," *Int. J. Heat Mass Transfer*, **47**, pp. 2417–2435.
[12] Mahan, G. D., and Woods, L. M., 1998, "Multilayer Thermionic Refrigeration," *Phys. Rev. Lett.*, **80**, pp. 4016–4019.
[13] Phelan, P. E., Song, Y., Nakabeppu, O., Ito, K., Hijikata, K., Ohmori, T., and Torikoshi, K., 1994, "Film/Substrate Thermal Boundary Resistance for an Er-Ba-Cu-O High-*T_C* Thin Film," *ASME J. Heat Transfer*, **116**, pp. 1038–1041.
[14] Phelan, P. E., 1998, "Application of Diffuse Mismatch Theory to the Prediction of Thermal Boundary Resistance in Thin-Film High-*T_C* Superconductors," *ASME J. Heat Transfer*, **120**, pp. 37–43.
[15] Chen, G., Tien, C. L., Wu, X., and Smith, J. S., 1994, "Thermal Diffusivity Measurement of GaAs/AlGaAs Thin-Film Structures," *ASME J. Heat Transfer*, **116**, pp. 325–331.
[16] Kim, E.-K., Kwun, S.-I., Lee, S.-M., Seo, H., and Yoon, J.-G., 2000, "Thermal Boundary Resistance at Ge₂Sb₂Te₅/ZnS:SiO₂ Interface," *Appl. Phys. Lett.*, **76**, pp. 3864–3866.
[17] Qiu, T. Q., and Tien, C. L., 1994, "Femtosecond Laser Heating of Multi-Layer Metals—I. Analysis," *Int. J. Heat Mass Transfer*, **37**, pp. 2789–2797.
[18] Qiu, T. Q., Juhasz, T., Suarez, C., Bron, W. E., and Tien, C. L., 1994, "Femtosecond Laser Heating of Multi-Layer Metals—II. Experiments," *Int. J. Heat Mass Transfer*, **37**, pp. 2799–2808.
[19] Smith, A. N., and Calame, J. P., 2004, "Impact of Thin Film Thermophysical Properties on Thermal Management of Wide Bandgap Solid-State Transistors," *Int. J. Thermophys.*, **25**, pp. 409–422.

- [20] Majumdar, A., Fushinobu, K., and Hijikata, K., 1995, "Effect of Gate Voltage on Hot-Electron and Hot-Phonon Interaction and Transport in a Submicrometer Transistor," *J. Appl. Phys.*, **77**, pp. 6686–6694.
[21] Zhang, Z., 2007, *Nano/Microscale Heat Transfer*, McGraw-Hill, New York.
[22] Chen, G., 2005, *Nanoscale Energy Transport and Conversion: A Parallel Treatment of Electrons, Molecules, Phonons, and Photons*, Oxford University Press, New York.
[23] Gray, D. E., 1972, *American Institute of Physics Handbook*, McGraw-Hill, New York.
[24] Cheeke, J. D. N., Ettinger, H., and Hebrall, B., 1976, "Analysis of Heat Transfer Between Solids at Low Temperatures," *Can. J. Phys.*, **54**, pp. 1749–1771.
[25] Little, W. A., 1959, "The Transport of Heat Between Dissimilar Solids at Low Temperatures," *Can. J. Phys.*, **37**, pp. 334–349.
[26] Swartz, E. T., and Pohl, R. O., 1989, "Thermal Boundary Resistance," *Rev. Mod. Phys.*, **61**, pp. 605–668.
[27] Kittel, C., 1996, *Introduction to Solid State Physics*, Wiley, New York.
[28] Vincenti, W. G., and Kruger, C. H., 2002, *Introduction to Physical Gas Dynamics*, Krieger, Malabar, FL.
[29] Snyder, N. S., 1970, "Heat Transport Through Helium II: Kapitza Conductance," *Cryogenics*, **10**, pp. 89–95.
[30] Stevens, R. J., Smith, A. N., and Norris, P. M., 2006, "Signal Analysis and Characterization of Experimental Setup for the Transient Thermoreflectance Technique," *Rev. Sci. Instrum.*, **77**, p. 084901.
[31] Hopkins, P. E., Stevens, R. J., and Norris, P. M., 2008, "Influence of Inelastic Scattering at Metal-Dielectric Interfaces," *ASME J. Heat Transfer*, **130**, p. 022401.
[32] Hopkins, P. E., Norris, P. M., Stevens, R. J., Beechem, T., and Graham, S., 2008, "Influence of Interfacial Mixing on Thermal Boundary Conductance Across a Chromium/Silicon Interface," *ASME J. Heat Transfer*, **130**, p. 062402.
[33] Poate, J. M., Tu, K. N., and Mayer, J. W., 1978, *Thin Films—Interdiffusion and Reactions*, Wiley, New York, pp. 1–12.
[34] Beechem, T. E., Graham, S., Hopkins, P. E., and Norris, P. M., 2007, "The Role of Interface Disorder on Thermal Boundary Conductance Using a Virtual Crystal Approach," *Appl. Phys. Lett.*, **90**, p. 054104.
[35] Kechrakos, D., 1991, "The Role of Interface Disorder in the Thermal Boundary Conductivity Between Two Crystals," *J. Phys.: Condens. Matter*, **3**, pp. 1443–1452.
[36] Ren, S.-F., Cheng, W., and Chen, G., 2006, "Lattice Dynamics Investigations of Phonon Thermal Conductivity of Si/Ge Superlattices With Rough Interfaces," *J. Appl. Phys.*, **100**, p. 103505.
[37] Stevens, R. J., Zhigilei, L. V., and Norris, P. M., 2007, "Effects of Temperature and Disorder on Thermal Boundary Conductance at Solid-Solid Interfaces: Nonequilibrium Molecular Dynamics Simulations," *Int. J. Heat Mass Transfer*, **50**, pp. 3977–3989.
[38] Kechrakos, D., 1990, "The Phonon Boundary Scattering Cross Section at Disordered Crystalline Interfaces: A Simple Model," *J. Phys.: Condens. Matter*, **2**, pp. 2637–2652.
[39] Prasher, R. S., and Phelan, P. E., 2001, "A Scattering-Mediated Acoustic Mismatch Model for the Prediction of Thermal Boundary Resistance," *ASME J. Heat Transfer*, **123**, pp. 105–112.
[40] Kozorezov, A. G., Wigmore, J. K., Erd, C., Peacock, A., and Poelaert, A., 1998, "Scattering-Mediated Transmission and Reflection of High-Frequency Phonons at a Nonideal Solid-Solid Interface," *Phys. Rev. B*, **57**, pp. 7411–7414.
[41] Stoner, R. J., and Maris, H. J., 1993, "Kapitza Conductance and Heat Flow Between Solids at Temperatures From 50 to 300 K," *Phys. Rev. B*, **48**, pp. 16373–16387.
[42] Abeles, B., 1963, "Lattice Thermal Conductivity of Disordered Semiconductor Alloys at High Temperatures," *Phys. Rev.*, **131**, pp. 1906–1911.
[43] Majumdar, A., and Reddy, P., 2004, "Role of Electron-Phonon Coupling in Thermal Conductance of Metal-Nonmetal Interfaces," *Appl. Phys. Lett.*, **84**, pp. 4768–4770.
[44] Kaganov, M. I., Lifshitz, I. M., and Tanatarov, L. V., 1957, "Relaxation Between Electrons and the Crystalline Lattice," *Sov. Phys. JETP*, **4**, pp. 173–178.
[45] Qiu, T. Q., and Tien, C. L., 1993, "Size Effects on Nonequilibrium Laser Heating of Metal Films," *ASME J. Heat Transfer*, **115**, pp. 842–847.
[46] Qiu, T. Q., and Tien, C. L., 1993, "Heat Transfer Mechanisms During Short-Pulse Laser Heating of Metals," *ASME J. Heat Transfer*, **115**, pp. 835–841.
[47] Hostetler, J. L., Smith, A. N., Czajkowsky, D. M., and Norris, P. M., 1999, "Measurement of the Electron-Phonon Coupling Factor Dependence on Film Thickness and Grain Size in Au, Cr, and Al," *Appl. Opt.*, **38**, pp. 3614–3620.
[48] Chen, Y., Li, D., Yang, J., Wu, Y., Lukes, J., and Majumdar, A., 2004, "Molecular Dynamics Study of the Lattice Thermal Conductivity of Kr/Ar Superlattice Nanowires," *Physica B*, **349**, pp. 270–280.
[49] Kosevich, Y. A., 1995, "Fluctuation Subharmonic and Multiharmonic Phonon Transmission and Kapitza Conductance Between Crystals With Very Different Vibrational Spectra," *Phys. Rev. B*, **52**, pp. 1017–1024.
[50] Lyeo, H.-K., and Cahill, D. G., 2006, "Thermal Conductance of Interfaces Between Highly Dissimilar Materials," *Phys. Rev. B*, **73**, p. 144301.

- [51] Hopkins, P. E., and Norris, P. M., 2007, "Effects of Joint Vibrational States on Thermal Boundary Conductance," *Nanoscale Microscale Thermophys. Eng.*, **11**, pp. 247–257.
- [52] Hopkins, P. E., and Norris, P. M., 2006, "Thermal Boundary Conductance Response to a Change in Cr/Si Interfacial Properties," *Appl. Phys. Lett.*, **89**, p. 131909.
- [53] Hopkins, P. E., and Norris, P. M., 2009, "Relative Contributions of Inelastic and Elastic Diffuse Phonon Scattering to Thermal Boundary Conductance Across Solid Interfaces," *ASME J. Heat Transfer*, **131**, p. 022402.
- [54] Huberman, M. L., and Overhauser, A. W., 1994, "Electronic Kapitza Conductance at a Diamond-Pb Interface," *Phys. Rev. B*, **50**, pp. 2865–2873.